京都大学学術情報リポジトリ
KURENAI 紅
Kyoto University Research Information Repository

京都大学
KYOTO UNIVERSITY

Title	Natural convection heat transfer from horizontal rod bundles in liquid sodium. Part 1: Correlations for two parallel horizontal cylinders based on experimental and theoretical results
Author(s)	Hata, Koichi; Takeuchi, Yuto; Hama, Katsuhiko; Shiotsu, Masahiro
Citation	Journal of Nuclear Science and Technology (2014), 52(2): 214-227
Issue Date	2014-04-04
URL	http://hdl.handle.net/2433/198282
Right	The Version of Record of this manuscript has been published and is available in Journal of Nuclear Science and Technology (2014) http://www.tandfonline.com/10.1080/00223131.2014.943317.
Type	Journal Article
Textversion	author

Kyoto University

ARTICLE

Natural convection heat transfer from horizontal Rod bundles in liquid sodium

Part 1 : Correlations for two parallel horizontal cylinders based on experimental and theoretical results

Koichi Hata[a]*, Yuto Takeuchi[a], Katsuhiko Hama[b] and Masahiro Shiotsu[b]

[a] *Institute of Advanced Energy, Kyoto University, Gokasho, Uji, Kyoto 611-0011, Japan*

[b] *Dept. of Energy Science and Technology, Kyoto University, Sakyo-ku, Kyoto 606-8501, Japan*

Natural convection heat transfer coefficients on two parallel horizontal test cylinders in liquid sodium were obtained experimentally and theoretically for various setting angles, γ, between vertical direction and the plane including both of these cylinder axis, over the range of zero to 90°. Both test cylinders are 7.6 mm in diameter and 50 mm in heated length with the ratio of the distance between each cylinder axis to the cylinder diameter, *S/D*, of 2. Theoretical equations for laminar natural convection heat transfer from the two horizontal cylinders were numerically solved for the same conditions as the experimental ones. The average Nusselt numbers *Nu* on the cylinders obtained experimentally were compared with the corresponding theoretical values on the *Nu* versus modified Rayleigh number R_f [$=Gr^*Pr^2/(4+9Pr^{1/2}+10Pr)$] graph. The experimental values of *Nu* for the upper cylinder are about 20 % lower than those for the lower cylinder at γ=0° for the range of R_f tested here. The value of *Nu* for the upper cylinder becomes higher and approaches that for the lower cylinder with the increase in γ over range of 0 to 90°: the values for each cylinder agree with each other at γ=90°. The values of *Nu* for the lower cylinder at each γ are almost in agreement with those for a single cylinder. The theoretical values of *Nu* on two cylinders except those for R_f<4 at γ=0° are in agreement with the experimental data at each γ with the deviations less than 15 %. Correlations for two

cylinders were obtained as functions of *S/D* and γ based on the theoretical solutions. A combined correlation for multi-cylinders in a vertical array based on the correlations for two cylinders was developed. The values by the correlation agree with the theoretical solution for the multi-cylinders for R_f ranging from 4.7 to 63 within 10 % difference.

Keywords ; natural convection heat transfer; liquid sodium; horizontal rod bundle

*Corresponding author. Email: hata@iae.kyoto-u.ac.jp

1. Introduction

There have been many studies on natural convection heat transfer. Most of them are for single horizontal cylinders, and correlations for gases and non-metallic and metallic liquids have been reported. The correlations based on boundary layer approximation were found to become inapplicable in the region of low Rayleigh numbers where curvature effect on heat transfer is no longer negligible. Several correlations based on experimental data for a wide range of Rayleigh numbers were presented [1, 2]. Some of the authors [3] presented the correlation based on rigorous numerical solutions for a wide range of R_f and Pr.

There have been a few works on interactions between two or more horizontal cylinders in natural convection. Marsters [4] carried out a study of three, five and nine horizontal cylinders in a vertical array in air. They have found that for closely spaced arrays, individual tube Nusselt numbers are smaller than for a single cylinder, and for wide spacings individual tube Nusselt numbers are higher than for a single cylinder. Lieberman and Gebhard [5] have conducted experiments in air on the interactions of heated wires arranged in a plane array. The array could be oriented so that its plane made angles of 0°, 30°, 60° and 90° with the vertical. Their data were for the wire spacings ranging from 37.5 diameters to 225 diameters.

Study on the correlation for natural convection heat transfer from a horizontal rod bundle in liquid sodium is important as a database for the design of a heat exchanger in a fast breeder reactor in relation to decay heat removal at a loss of flow accident. However, there is no reliable correlation even for two horizontal cylinders with various setting angles between the plane including the cylinders and vertical direction and for the distance between the cylinders.

The objectives of present study are: (1) to obtain the experimental data of natural convection heat transfer from each of two horizontal cylinders systematically for a wide range of heat flux at the setting angles γ over the range of zero to 90°, (2) to obtain the numerical solutions of the average and local Nusselt numbers on two horizontal cylinders from a theoretical laminar natural convection equations for the same experimental conditions, (3) to

compare experimental results with corresponding theoretical values to confirm the reliability of both results, (4) to present a correlation to describe the effects of γ and *S/D* on natural convection heat transfer on two cylinders based on the theoretical solution, and (5) to present a combined correlation for multi-cylinders in a vertical array based on the correlations for two cylinders.

Extension of this work to multi-rod bundles is performed in Part 2 of this paper.

2. Apparatus and Method

Experimental apparatus consists of a test vessel containing a test heater, a vapor condenser, an inert gas supply, a vacuum system, a sodium purification system and instrumentation. Explanations on major parts of the apparatus are as follows.

The test vessel is shown schematically in **Figure 1**. It is a cylindrical vessel of 30 cm in inner diameter and 70 cm in height containing liquid sodium of about 30 liter. Measuring device of the vertical temperature distribution in the liquid consisting of several K type thermocouples and one standard PR(13 %) thermocouple is mounted vertically by using a flange on the top of the vessel. Two test cylinders are mounted horizontally at the height of about 170 mm from the inner bottom of the vessel. Lower part of the vessel up to the height of 500 mm is in an electric furnace whose power is PID controlled to keep the liquid in the vessel at a desired temperature.

< Figure 1 >

The two test cylinders used in the experiment are shown in **Figure 2**. Both test cylinders have the diameter of 7.6 mm and heated length of 50 mm. They are mounted on a flange with the *S/D* value of 2. Each test cylinder is a nickel sheathed once-through current type with a spiral tantalum heating element one end of which is connected to an electrode with a potential tap, the other end being grounded to liquid sodium. Boron nitride is used as the electrical insulation material. Eight 0.5 mm diameter K type thermocouples are embedded in the

grooves on each test cylinder surface, brazed and surface finished. The flange for these two horizontal cylinders can be rotated every 30°. The angle between the vertical direction and the plane including both of the cylinders axis plane is called in this work the setting angle γ. γ=0° means the location where the upper cylinder is just above the lower one, and γ=90° means that one is just beside the other. The thermocouple locations are shown in **Figure 3 (a) to (d)**, for γ=0, 30, 60, and 90°, respectively.

< Figure 2 >

< Figure 3 (a) to (d) >

The heating current to each test cylinder is supplied by a power amplifier which can supply a direct current of up to 300 amperes at a power level of 10 kW. The input signal of the power amplifier is controlled by a digital computer so that the heat generation rate in the test cylinder agrees with a desired value. In this work, heat inputs to the two test cylinders are equally given.

Signal voltages expressing the heating current and the terminal voltage of the test heater, heater surface temperatures and bulk liquid temperatures are sent to each insulated amplifier, and the amplified signals are led to a digital computer through AD converters. The heat flux, q, is calculated from the measured values of the heating current and the terminal voltage. The measured output voltage for each thermocouple is converted to temperature by using the voltage-temperature relation preliminary calibrated for each thermocouple. The calibration was performed in sodium by using a standard precision PR(13%) thermocouple. The heater wall temperature, T_w, was calculated from the measured temperature at 0.25 mm inner positions from the surface by solving the thermal conduction equation in the heater sheath supposing a uniform surface heat flux, q. Measurement error was estimated to be ±1 % in the heat flux and ±2 K in the heater wall temperature. The edge effect on natural convection heat transfer from both cylinders was estimated based on the theoretical solution for 3-dimensional natural convection model to be about 5 % and 2 % for the upper and lower cylinders

respectively at the outermost thermocouple locations of 9 mm from both ends of heated section, and negligibly small at other thermocouple locations.

Experiments were performed as follows. After charging up liquid sodium to the test loop from the storage tank, sodium was purified to an oxide content of less than 5 ppm by circulating it through a cold trap at the temperature of 390 K for about 8 hours. Then, the circulation pump was shut off and liquid level in the test vessel was adjusted to about 300 mm above the horizontal test cylinders. Liquid temperature was raised and kept constant at 673 K by using the electric furnace. Pressure of Argon cover gas was kept constant at around atmospheric. After the system has reached a steady state with negligible vertical temperature distribution in the liquid, electric current to the test cylinders was gradually raised to a desired heat flux level. The heat flux was kept for 76 s during which the measurements were made in the time intervals of 0.1 s.

3. Experimental Results and Discussion

3.1 The Correlation Previously Obtained for a Single Horizontal Cylinder

The correlation of natural convection heat transfer from single horizontal cylinders based on rigorous numerical solutions for natural convection without the boundary layer approximation previously obtained by some of the authors [3] is firstly explained. The theoretical values of *Nu* for a wide range of *Ra* for *Pr* ranging from 0.005 to 10 were expressed by a single curve on the *Nu* versus modified Rayleigh number R_f [$=Gr^* Pr^2/(4+9Pr^{1/2}+10Pr)$] graph. The theoretical *Nu* values on a horizontal cylinder obtained with boundary layer approximation for *Pr* from near zero to infinity can be expressed as a single line, ($Nu=1.03\ R_f^{1/5}$), on *log Nu* versus *log* R_f graph. This is the asymptotic line to which true *Nu* approaches with the increase in R_f. The following correlation for *Nu* was given as a function of R_f by least square fitting within ±4% error.

$$\mathrm{Nu} = 10^{z} \qquad (1)$$

where

$$z = 0.193385 + 0.145037 \log R_f + 0.664323 \times 10^{-2} (\log R_f)^2 - 0.232432 \times 10^{-3} (\log R_f)^3 - 0.238613 \times 10^{-4} (\log R_f)^4 \quad (2)$$

The correlation based on the theoretical values expressed the authors' experimental data on single horizontal cylinders of 7.6 and 10.7 mm in diameter in liquid sodium for a wide range of R_f within ±10 % deviation and many conventional experimental data obtained by other workers on various diameter cylinders in various liquids and gases with *Pr* from 0.005 to 6.7, for R_f from about 10^{-8} to 10^{6} within ±20 % deviation.

The correlation was also compared with existing correlations. The values by Churchil and Chu's correlation [1] for *Pr* ranged over 0.005 to 10 were lower than those by Equation (1) for $R_f > 10^{-4}$ with the maximum deviation of 20 %. The values agreed with the correlation at around $R_f = 10^{-4}$ and then became far higher than that by Equation (1) with decreasing R_f from 10^{-4}. The values predicted by Raithby and Hollands' correlation [2] were in good agreement with those by Equation (1) in most of the R_f range. However, in the range ($10^{-6.5} < R_f < 10^{-1.5}$), the values by their correlation were about 10 % higher than those predicted by Equation (1) and in good agreement with conventional experimental data in the range. It was suggested that the correlations based on experimental data had a possibility of containing the same order of errors as the experimental errors. In this work, average heat transfer coefficients on two cylinders measured for a wide range of heat input and corresponding theoretical value are plotted to compare with each other on a *Nu* versus R_f graph.

3.2 Experimental Results of Heat Transfer Coefficients for Upper and Lower Cylinders at Each Setting Angle

Natural convection heat transfer coefficients on two horizontal 7.6 mm-diameter cylinders at the same heat input were measured. Experimental conditions are tabulated in **Table 1**.

< Table 1 >

The experimental results for the two cylinders are compared with the rigorous solutions for the theoretical model of laminar natural convection heat transfer from two parallel horizontal cylinders with a uniform heat flux obtained for the same conditions as the experimental ones considering the temperature dependence of thermo-physical properties by using a commercial CFD cord PHOENICS [6]. Outline of the theoretical equations and calculation method are shown in Appendix 1. **Table 2** shows the parameters used for the calculation.

< Table 2 >

3.2.1 In case of the setting angle γ=0°

Experimental results of average heat transfer coefficients in case of γ=0° (upper cylinder is just above the lower one) are plotted on *Nu* vs. R_f graph in **Figure 4**. Open circles show the results for the lower cylinder and open triangles show those for the upper cylinder. As can be seen in the figure, the value of *Nu* for the upper cylinder at each R_f is about 20 % lower than that for the lower cylinder. The *Nu* values for single cylinders predicted by Equation (1) are shown in the figure as a solid curve for comparison. The experimental results of *Nu* for the lower cylinder are almost in agreement with the curve for whole range of R_f tested here. Numerical solutions of *Nu* for the lower and upper cylinders are also shown in the figure as solid circles and solid triangles, respectively. The numerical solution for the lower cylinder is from about 8 % to 17 % lower than the experimental one. The solution for the upper cylinder is about 15 % lower than the experimental one for $R_f \geq 4$; the difference becomes larger with the decrease in R_f from 4.

< Figure 4 >

Figure 5 shows the peripheral distribution of local Nusselt numbers Nu_θ on the upper and lower cylinders for the data shown in **Figure 4** at R_f=6.9 (q=1.0 × 10^6 W/m^2) in comparison with the numerical solutions of Nu_θ for a single cylinder. The Nu_θ is the Nusselt

number at the angle θ from the bottom (θ=0° at the bottom). The data for the lower and upper cylinders are shown as solid circles and solid triangles, respectively with the fluctuation range. Considering the symmetry of the phenomena in case of γ=0°, measured values on the left hand side are plotted at a corresponding angle on the positive θ region. As can be seen in the figure, Nu_θ data for the lower cylinder almost agree with the values for a single cylinder. On the contrary, Nu_θ data for the lower part of the upper cylinder ($\theta \leq$90°) are affected by the thermal boundary layer of the lower cylinder: they become lower than those for the lower cylinder and single cylinder with the decrease in θ from around 90°. The Nu_θ at θ=0° is about 63 % of that for the lower cylinder. Numerical solutions of the Nu_θ for the lower and upper cylinders are also shown as open circles and open triangles, respectively, in the figure. The theoretical Nu_θ for the lower cylinder are almost in agreement with the corresponding experimental data and with the curve for the single cylinder. However, those for the upper cylinder are about 15 % lower than the corresponding experimental data for all the θ range. That causes the theoretical *Nu* values about 15 % lower than the corresponding experimental data as mentioned above.

< Figure 5 >

3.2.2 In case of the setting angle γ=30°

Average heat transfer coefficients in case of γ=30° are shown in **Figure 6**. The *Nu* values for the upper cylinder are about 20 % lower than those for the lower cylinder for the R_f lower than 1.3. They approach the latter values with the R_f becoming higher than 1.3, and finally arrive at the value about 14 % lower than the latter values at R_f =14. Numerical solutions of the *Nu* for the lower and upper cylinders are also shown in the figure for comparison. The solutions for the lower and upper cylinders are about 10 % lower than the average of the corresponding experimental data.

< Figure 6 >

Figure 7 shows the typical distribution of Nu_θ on the upper and lower cylinders for the

data shown in **Figure 6** at R_f=6.7. As can be seen in the figure, Nu_θ data for the lower cylinder almost agree with the values for a single cylinder, although the data are somewhat scattered. On the contrary, Nu_θ data for the upper cylinder in the positive θ region (right hand side of the cylinder facing the lower cylinder) are lower than those for the lower cylinder and single cylinder being affected by the thermal boundary layer of the lower cylinder. Numerical solutions of Nu_θ for the lower and upper cylinders are shown as open circles and open triangles, respectively, in the figure. The solutions for the lower and upper cylinders are almost in agreement with the corresponding experimental data.

< Figure 7 >

3.2.3 In case of the setting angle γ=60°

The data of *Nu* in case of γ=60° are shown in **Figure 8**. The *Nu* values for the upper cylinder are about 14 % lower than those for the lower cylinder. The theoretical solutions of *Nu* for the lower and upper cylinders are also shown in the figure for comparison. The solutions for the lower cylinder almost agree with the corresponding experimental data, and those for the upper cylinder are about 6 % higher than the average of corresponding experimental data.

< Figure 8 >

Figure 9 shows the distribution of Nu_θ on the upper and lower cylinders for the data shown in **Figure 8** at R_f =6.7. As seen from the figure, Nu_θ data for the lower cylinder agree with the value for a single cylinder at θ around 0°, and they become higher and lower than the corresponding values for a single cylinder with increasing and decreasing θ from the value, respectively. Namely, the heat transfer in the left side of the lower cylinder facing the upper cylinder is disturbed and that in the opposite side is enhanced by the upper cylinder. On the other hand, Nu_θ in the positive θ region of the upper cylinder (right side of the cylinder facing the lower cylinder) are lower than those for the lower cylinder, although the data in the negative θ region are almost in agreement with those for a single cylinder. The theoretical

solutions of Nu_θ for the lower and upper cylinders are shown in the figure. In comparison with the experimental data, the solutions of Nu_θ for the lower cylinder agree with the experimental data at θ=0° but they are higher and lower than the experimental data in the negative and positive range of θ, respectively. These differences compensate with each other and the theoretical *Nu* values for the lower cylinders are almost in agreement with the experimental data as mentioned above. The solutions of Nu_θ for the upper cylinder almost agree with the experimental data in the positive θ range but they are 11 % at θ=-30°, 15 % at θ=-90° and 32 % at θ=-120° higher than the experimental data in the negative θ range. These differences cause the *Nu* higher than the experimental data.

< Figure 9 >

3.2.4 In case of the setting angle γ=90°

The data of *Nu* in case of γ=90° (one cylinder is just beside the other) are shown in **Figure 10**. As the peripheral distribution of local surface temperatures on one cylinder is almost symmetrical to that on the other cylinder, *Nu* are obtained based on the measured local surface temperatures on both cylinders. The *Nu* value at R_f=0.1 is about 26 % lower than the curve for a single cylinder; it increases and gradually approaches the curve with the increase in R_f and almost agrees with the curve for $R_f \geq 5$. It should be noted that, in the cases of γ=60° and 90°, *Nu* for both cylinders become lower than the corresponding values for a single cylinder in the lower R_f range due to the mutual effect. On the contrary, in the cases of γ=0° and 30°, *Nu* for the lower cylinder almost agree with those for a single cylinder, and only the heat transfer from upper cylinder is disturbed by the mutual effect. The theoretical solutions of *Nu* are also shown in **Figure 10** for comparison. They are in agreement with the corresponding experimental data within the scattering range.

< Figure 10 >

Figure 11 shows the typical distribution of Nu_θ on the left side cylinder (which is the upper cylinder for γ < 90°) for the data shown in **Figure 10** at R_f=6.7. As the peripheral

distribution of heat transfer coefficients on one cylinder is almost symmetrical to that for the other cylinder, Nu_θ data on the right side cylinder are also plotted in the figure at the corresponding θ. Though the Nu_θ data in the negative and positive θ range are slightly higher and lower than the values for a single cylinder, respectively, they are almost in agreement with those for a single cylinder. The theoretical solutions of Nu_θ are also shown in the figure. The solution almost describes the angular distribution of the Nu_θ.

< Figure 11 >

3.3 Effect of the Setting Angle

The experimental data of Nu for R_f =0.448, 4.6, and 13.8 are shown versus the setting angle γ in **Figures 12 (a)**, **12 (b)**, and **12 (c)**, respectively, in comparison with the theoretical solution. The value for a single cylinder is also shown in each figure as a broken line. As shown in these figures, the experimental values of Nu for the upper cylinder are lower than those for the lower cylinder: the difference becomes smaller with the increase in γ and arrives at zero at γ=90°. For the low heat flux corresponding to R_f=0.448 shown in **Figure 12 (a)**, the experimental data for the lower cylinder at γ=0°, 30° are almost in agreement with, and those for γ larger than 60° are about 20 % lower than the value for a single cylinder. For the heat flux ten times higher (R_f=4.6) shown in **Figure 12 (b)**, the experimental data for the lower cylinder are almost in agreement with the value for a single cylinder for all the γ range. For the heat flux further about three times higher (R_f=13.8) shown in **Figure 12 (c)**, the experimental data for the lower and upper cylinders have maximum values at γ=30°. These maximum values are not predicted by the theoretical solutions and are about 15 % higher than the predicted values.

< Figures 12 (a), 12 (b), and 12 (c) >

4. Correlations for Two Cylinders

The numerical solutions agreed with the *Nu* data within 15 % difference. In this section, the correlations for two cylinders including the effects of γ and *S/D* is presented based on the numerical solutions. Then a combined correlation for multi-cylinders in a vertical array with a constant *S/D* is developed based on the correlations for two cylinders.

4.1 Estimation of S/D Effect

The effect of *S/D* on natural convection heat transfer from each of the two horizontal cylinders was estimated based on the numerical solutions of the above mentioned theoretical model. The calculations were made for the *S/D* of 1.5, 2.0, 3.0 and 4.0 at the γ of 0°, 30°, 60° and 90° for R_f ranging from 0.064 to 13.8. The ratios of the calculated *Nu* to those for a single cylinder given by Equation (1) at the same condition, Nu/Nu_{sc}, are shown versus γ with *S/D* as a parameter in **Figures 13 (a), 13 (b) and 13 (c)** for the R_f values of 0.448, 4.6 and 13.8, respectively. The open symbols show the values for the lower cylinder and the solid symbols show those for the upper cylinder. As can be seen in these figures, the values of Nu/Nu_{sc} for the upper cylinder are lower for the lower values of *S/D*, γ and R_f. The values of Nu/Nu_{sc} for the lower cylinder show nearly the same trend of dependence on *S/D*, γ and R_f, although they are far higher than the corresponding values for the upper cylinder.

< Figures 13 (a), 13 (b) and 13 (c) >

4.2 Correlations for Two Cylinders

The calculated values of Nu/Nu_{sc} for the upper and lower cylinders are approximately expressed by the following correlations.

For the upper cylinder:

$$Nu / Nu_{SC} = 1 - 0.60 \exp[-AR_f^m (S / D)] \qquad (3)$$

where

$$A = 0.29 + 6.8 \times 10^{-3}\gamma, \quad m = 0.12 + 1.67 \times 10^{-3}\gamma$$

For the lower cylinder:

$$Nu / Nu_{SC} = 1 - C\exp[-KR_f^n (S/D)] \tag{4}$$

where

$$C = 0.4 + 2.2 \times 10^{-3}\gamma,$$
$$K = 0.56 + 0.34(S/D)\sin\gamma \quad : \quad 0 \le \gamma \le \arcsin(D/S)$$
$$= 0.9 \quad : \quad \gamma > \arcsin(D/S)$$
$$n = 0.16 + 1.2 \times 10^{-3}\gamma$$

The curves of Nu/Nu_{sc} for upper and lower cylinders derived from these correlations are shown in **Figures 13 (a) to (c)** for comparison. They are in agreement with the numerical solutions for the upper and lower cylinders within 9 % error.

4.3 Application of the Correlations for Two Cylinders to Multi-cylinders

It was intended to present a combined correlation for multi-cylinders in a vertical array with a constant *S/D* based on the correlations for two cylinders. Each horizontal cylinder consisting the vertical array are numbered sequentially from i=1 (lowermost cylinder) to $i=N_m$ (uppermost one).

The combined correlation is as follows:

$$\left[Nu / Nu_{SC}\right]_{i=a} = \prod_{i=1}^{a-1}[1 - 0.60\exp\{-AR_f^m (a-i)S/D\}] \times \prod_{i=a}^{N_m - 1}[1 - C\exp\{-KR_f^n (N_m - i)S/D\}] \tag{5}$$

where the Nu/Nu_{sc} value for a cylinder with $i=a$ is given by multiplying the mutual effects between the cylinder and other lower and upper cylinders predicted by Equations (3) and (4).

The theoretical solutions of natural convection heat transfer from five and nine horizontal cylinders in a vertical array with *S/D* of 2 were obtained. The values of Nu/Nu_{sc} for each cylinder are shown versus cylinder number N in **Figures 14 and 15** with R_f as a

parameter. As shown in the figure, the value of Nu/Nu_{sc} at each cylinder is higher for higher R_f, and the value for a certain R_f is lower for upper cylinder. The values of Nu/Nu_{sc} for each cylinder derived from the combined correlation are shown as a curve for each value of R_f in the figure for comparison. The values for R_f higher than 4.67 are within 10 % of the theoretical solution, and those for the R_f of 1.29 and 0.45 are about 18 and 26 %, respectively, lower than the solution.

< Figures 14 and 15 >

4.4 Comparison of the Correlation with Other Worker's Experimental Data on Multi-Cylinders in Air

The correlation for multi-cylinders in a vertical array including the effects of R_f , γ and S/D may be applicable to the experimental data in other liquids and gases because the correlation is based on the Nu_{sc} derived from the general correlation of natural convection heat transfer for a single cylinder and R_f is a generalized Rayleigh number. The correlation was compared with Marsters' experimental data [4] for five cylinders in a vertical array consisting S/D=2 in air.

Experimental data for each cylinder are shown in **Figure 16** with R_f as a parameter. The trend of Nu/Nu_{sc} for R_f and N is almost similar to the results of liquid sodium shown in **Figure 14**. The values of Nu/Nu_{sc} for each value of R_f derived from the correlation for multi-cylinders are shown as an individual curve for comparison. This correlation predicts the experimental data for five cylinders in air within 16 % difference.

< Figures 16 >

It is expected from these comparisons that the combined correlation based on the correlations for two cylinders may be applicable to multi-cylinders in 2 dimensional arrays in liquid sodium, although some modifications may be necessary. In Part 2 of this work, natural convection heat transfer from multi-rod bundles is numerically analyzed in liquid sodium and

a generalized correlation for multi-rod bundles is developed.

5. Summary and Conclusions

Experimental data of natural convection heat transfer on two horizontal cylinders with a uniform heat flux were obtained systematically for a wide range of Rayleigh number at the setting angles of the cylinders, γ, over the range of 0° to 90°.

The data of *Nu* for the upper cylinder are about 20 % lower than those for the lower cylinder at γ=0°. The values of *Nu* for the upper cylinder become higher and approach those for the lower cylinder with the increase in γ to 90°.

Theoretical solutions for the same conditions as the experimental ones were obtained. The experimental data for each cylinder are in agreement with the corresponding theoretical ones within 15 % difference.

The theoretical values of *Nu* on the cylinders with the *S/D* values ranging from 1.5 to 4 were obtained for the various angles of γ.

The correlations to express the natural convection heat transfer from two cylinders for the values of γ and *S/D* were presented based on the theoretical values.

The combined correlation for multi-cylinders in a vertical array based on the correlations for upper and lower cylinders was presented.

Nomenclature

A = parameter in Equation (3)

C = parameter in Equation (4)

D = cylinder diameter, m

Gr^* = $g \beta q D^4/\lambda \nu^2$, Grashof number for constant heat flux

g = acceleration of gravity, m/s^2

K = parameter in Equation (4)

m = exponent in Equation (3)

N = cylinder number

N_m = total number of cylinder

Nu = average Nusselt number

Nu_{sc} = average Nusselt number for single cylinder

Nu_θ = local Nusselt number at the position specified by the angle at the circumference

n = exponent in Equation (4)

Pr = Prandtl number

q = heat flux, W/m^2

Ra^* = Gr^*Pr, Rayleigh number for constant heat flux

R_f = $Gr^*Pr^2/(4+9Pr^{1/2}+10Pr)$, modified Rayleigh number

S = distance between the center axis of two parallel horizontal cylinders, m

T_0 = bulk liquid temperature, K

T_w = heater wall temperature, K

β = volumetric expansion coefficient, K^{-1}

γ = setting angle of the two horizontal cylinders, deg

θ = peripheral angle from the bottom of the cylinder, deg

λ = thermal conductivity, W/(m K)

ν = kinematic viscosity, m^2/s

References

[1] Churchil SW, Chu HHS, Correlating Equations for Laminar and Turbulent Free Convection from a Horizontal Cylinder. Int. J. Heat Mass Transfer. 1975; 18: 1049-1053.

[2] Raithby GD, Hollands KGT, Natural Convection. in: Handbook of Heat Transfer Fundamentals: MacGraw Hill, New York; 1985. p.6-1 - 6-94.

[3] Takeuchi Y, Hata K, Shiotsu M, Sakurai A, A General Correlation for Natural Convection

Heat Transfer from Horizontal Cylinders in Liquids and Gases. General Papers in Heat Transfer, ASME HTD-Vol.204. 1992: 183-189.

[4] Marsters G.F, Arrays of Heated Horizontal Cylinders in Natural Convection. Int. J. Heat Mass Transfer. 1972; 15: 921-933.

[5] Lieberman J, Gebhard B, Interactions in Natural Convection from an Array of Heated Elements, Experimental. Int. J. Heat Mass Transfer. 1968 12; 1385-1396.

[6] Spalding DB, The PHOENICS Beginner's Guide. Pub. by CHAM: UK; 1991.

[7] Patankar SV, Numerical Heat Transfer and Fluid Flow. Hemisphere Pub. Corp.: New York; 1980.

Appendix 1

Theoretical solution of laminar natural convection equations

A.1 Fundamental Equations

The unsteady laminar two dimensional basic equations in boundary fitted coordinates as shown in **Figures 17 (a) and (b)** for γ=0°, and **Figures 18 (a) and (b)** for γ =30° are described as follows.

< Figures 17 (a) and (b) >

< Figures 18 (a) and (b) >

(Continuity Equation)

$$\frac{\partial \rho}{\partial t} + \frac{\partial}{\partial x}(\rho u) + \frac{\partial}{\partial z}(\rho w) = 0 \qquad (6)$$

(Momentum Equation)

$$\frac{\partial}{\partial t}(\rho u) + \frac{\partial}{\partial x}(\rho u u) + \frac{\partial}{\partial z}(\rho w u) = -\frac{\partial P}{\partial x} + \frac{\partial}{\partial x}\tau_{xx} + \frac{\partial}{\partial z}\tau_{xz} \qquad (7)$$

$$\frac{\partial}{\partial t}(\rho w)+\frac{\partial}{\partial x}(\rho uw)+\frac{\partial}{\partial z}(\rho ww)=-\frac{\partial P}{\partial z}+\frac{\partial}{\partial x}\tau_{zx}+\frac{\partial}{\partial z}\tau_{zz}-\rho g \qquad (8)$$

(Energy Equation)

$$\frac{\partial}{\partial t}(\rho c_p T)+\frac{\partial}{\partial x}(\rho c_p uT)+\frac{\partial}{\partial z}(\rho c_p wT)=\frac{\partial}{\partial x}\{\frac{\lambda}{c_p}\frac{\partial}{\partial x}(c_p T)\}+\frac{\partial}{\partial z}\{\frac{\lambda}{c_p}\frac{\partial}{\partial z}(c_p T)\} \quad (9)$$

where

$$\tau_{xx}=2\rho\nu\frac{\partial u}{\partial x},\quad \tau_{zz}=2\rho\nu\frac{\partial w}{\partial z},\quad \tau_{xz}=\tau_{zx}=\rho\nu\left(\frac{\partial u}{\partial z}+\frac{\partial w}{\partial x}\right) \qquad (10)$$

u, *w* are the *x*, *z* components of a velocity vector, respectively.

The control volume discretization equations were derived from these equations by using the hybrid scheme [7]. The thermo-physical properties for each control volume are given as those at each volume temperature. The equations are numerically analyzed together with the following boundary conditions.

On the surfaces of cylinders: constant heat flux, and non-slip condition.

At the left and right outer boundary:

$$T=T_0,\quad \frac{\partial u}{\partial x}=0 \qquad \text{(for in-flow)}$$

$$\frac{\partial T}{\partial x}=0,\quad \frac{\partial u}{\partial x}=0 \qquad \text{(for out-flow)}$$

At the lower and upper boundary:

$$T=T_0,\quad \frac{\partial w}{\partial z}=0 \qquad \text{(for in-flow)}$$

$$\frac{\partial T}{\partial z}=0,\quad \frac{\partial w}{\partial z}=0 \qquad \text{(for out-flow)}$$

where T_0 is a bulk liquid temperature. The procedure for the calculation of the flow field is the

SIMPLE algorithm which stands for Semi-Implicit Method for Pressure-Linked Equations. Stepwise increase in surface heat flux was considered as an initial condition, and numerical calculation was continued until the steady-state was obtained. **Table 2** shows the parameters used for the calculation. Average heat transfer coefficient on the cylinder surface was obtained by averaging the calculated local temperatures at every 10° in θ. All the calculations were made by using the PHOENICS code [6].

List of figure captions

Figure 13 (b). Nu/Nu_{sc} versus γ for upper and lower cylinders with S/D as a parameter at R_f =4.6.

Figure 13 (c). Nu/Nu_{sc} versus γ for upper and lower cylinders with S/D as a parameter at R_f =13.8.

Figure 14. Nu/Nu_{sc} versus cylinder number N for N_m=5 with R_f as a parameter. Comparison with the predicted curves.

Figure 15. Nu/Nu_{sc} versus cylinder number N for N_m=9 with R_f as a parameter. Comparison with the predicted curves.

Figure 16. Comparison of correlation with Marsters' experimental data on five cylinders in air.

Figure 17 (a). Boundary fitted coordinates for γ=0°.

Figure 17 (b). Details of Boundary fitted coordinates for γ=0°.

Figure 18 (a). Boundary fitted coordinates for γ=30°.

Figure 18 (b). Details of Boundary fitted coordinates for γ=30°.

Table 1. Experimental Conditions.

System Pressure	85 ~ 94 kPa
Upper Cylinder Diameter (D)	7.6 mm
Upper Cylinder Length	50 mm
Lower Cylinder Diameter (D)	7.6 mm
Lower Cylinder Length	50 mm
S/D (S=Distance between Cylinder Axis)	2
γ (Setting Angle)	0°, 30°, 60°, 90°
Liquid Temperature	673 K
Liquid Head	300 mm
Heat Flux (q)	$2 \times 10^4 \sim 2 \times 10^6$ W/m^2 $q_{Upper\ Cylinder}=q_{Lower\ Cylinder}$
R_f ($=Gr^*Pr^2/(4+9Pr^{1/2}+10Pr)$)	0.1 ~14

Table 2. Parameters for Calculation.

2 Cylinders	
System Pressure	101.3 kPa
Upper Cylinder Diameter (D)	7.6 mm
Lower Cylinder Diameter (D)	7.6 mm
S/D (S=Distance between Cylinder Axis)	1.5, 2, 3, 4, 5
γ (Setting Angle)	0°, 10°, 30°, 60°, 90°
Liquid Temperature	673 K
Heat Flux (q)	1×10^4, 2×10^4, 7×10^4, 2×10^5, 7×10^5, 1×10^6, 2×10^6, 7×10^6 W/m^2
Gr^*	1.20×10^4, 2.41×10^4, 8.54×10^4, 2.49×10^5, 9.33×10^5, 1.38×10^6, 3.06×10^6, 1.43×10^7
$Ra^*(=Gr^*Pr)$	5.98×10 , 1.20×10^2, 4.24×10^2, 1.23×10^3, 4.50×10^3, 6.59×10^3, 1.42×10^4, 6.17×10^4
R_f $(=Gr^*Pr^2/(4+9Pr^{1/2}+10Pr))$	0.0637, 0.128, 0.448, 1.29, 4.60, 6.65, 13.8, 57.0
5 Cylinders	
System Pressure	101.3 kPa
Each Cylinder Diameter (D)	7.6 mm

S/D	2
γ (Setting Angle)	0°
Liquid Temperature	673 K
Heat Flux (q)	1×10^4, 2×10^4, 7×10^4, 2×10^5, 7×10^5, 1×10^6, 2×10^6, 7×10^6 W/m^2
Gr^*	1.20×10^4, 2.41×10^4, 8.54×10^4, 2.49×10^5, 9.33×10^5, 1.38×10^6, 3.06×10^6, 1.43×10^7
$Ra^*(=Gr^*Pr)$	5.98×10 , 1.20×10^2, 4.24×10^2, 1.23×10^3, 4.50×10^3, 6.59×10^3, 1.42×10^4, 6.17×10^4
R_f $(=Gr^*Pr^2/(4+9Pr^{1/2}+10Pr))$	0.0637, 0.128, 0.449, 1.29, 4.67, 6.78, 14.2, 63.1

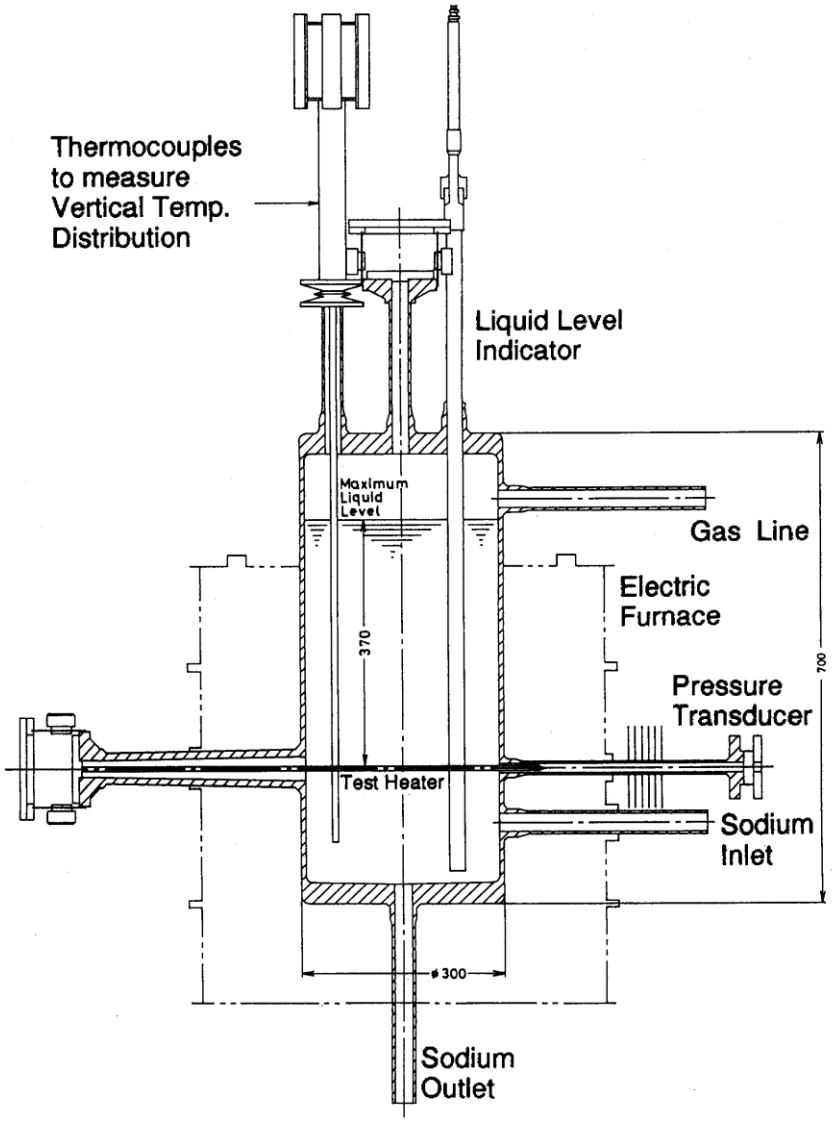

Figure 1. Schematic diagram of test vessel.

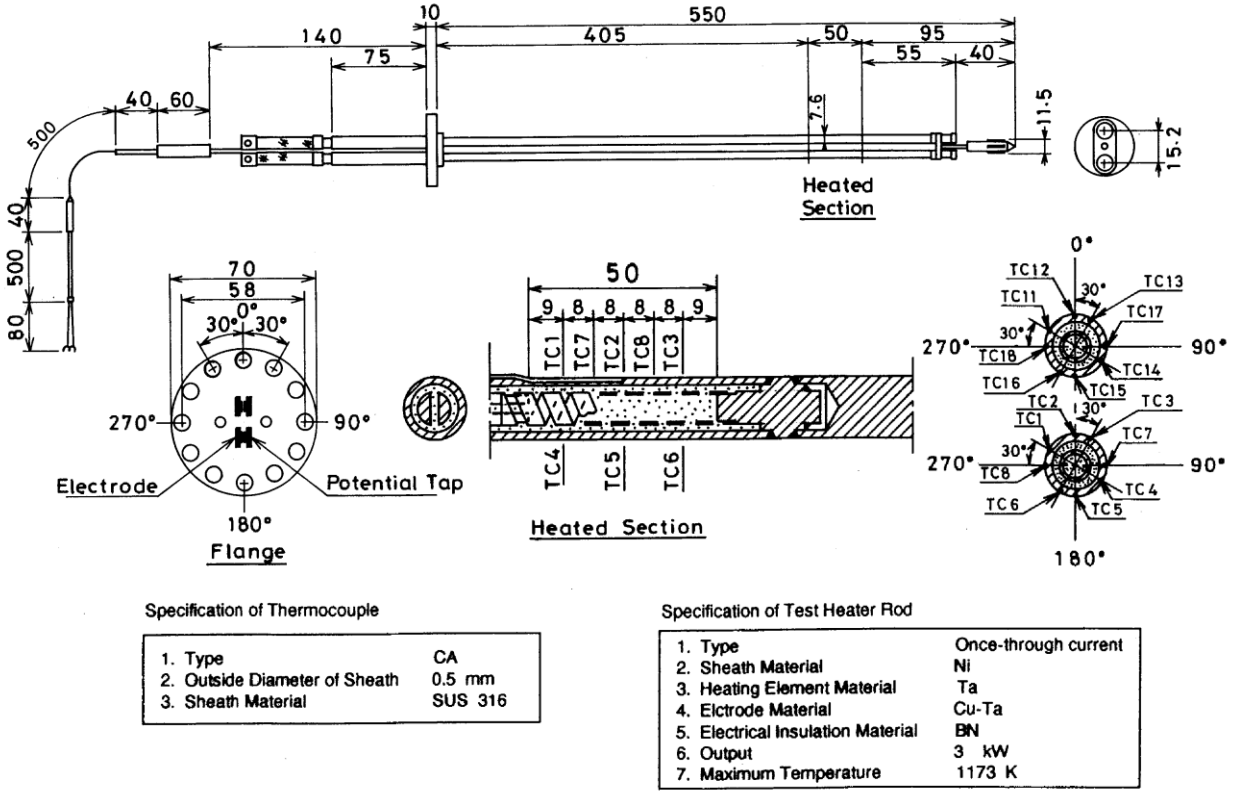

Specification of Thermocouple

1. Type	CA
2. Outside Diameter of Sheath	0.5 mm
3. Sheath Material	SUS 316

Specification of Test Heater Rod

1. Type	Once-through current
2. Sheath Material	Ni
3. Heating Element Material	Ta
4. Elctrode Material	Cu-Ta
5. Electrical Insulation Material	BN
6. Output	3 kW
7. Maximum Temperature	1173 K

Figure 2. Schematic diagram of two horizontal cylinders with *S/D*=2.

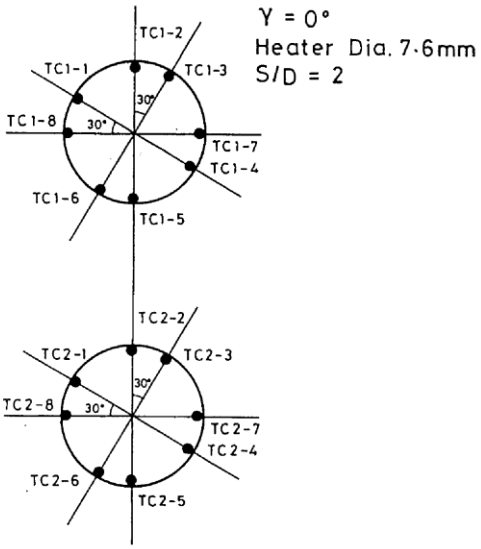

Figure 3 (a). Thermocouple locations for γ=0°.

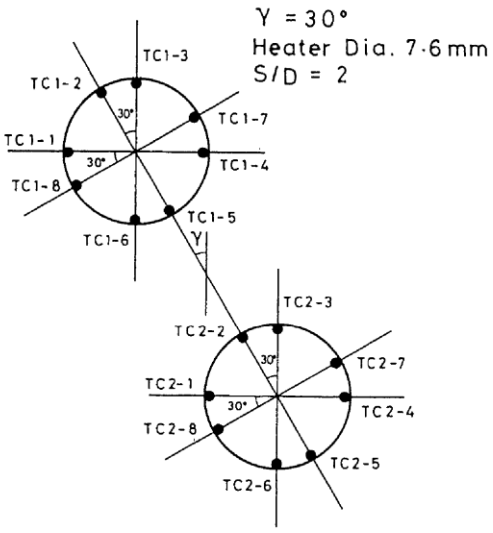

Figure 3 (b). Thermocouple locations for γ=30°.

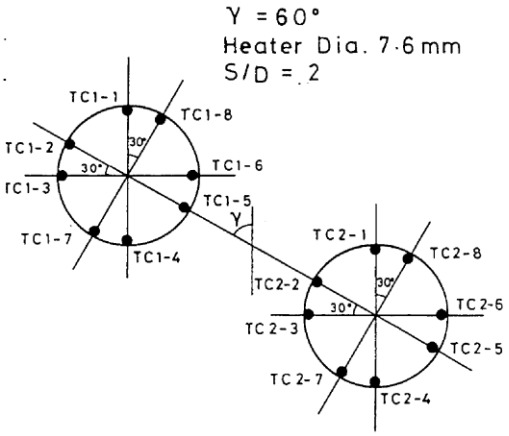

Figure 3 (c). Thermocouple locations for γ=60°.

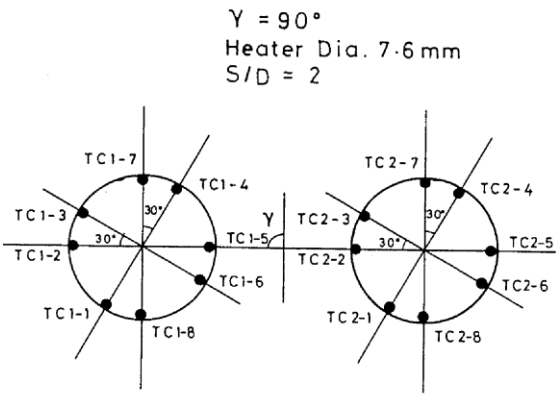

Figure 3 (d). Thermocouple locations for γ=90°.

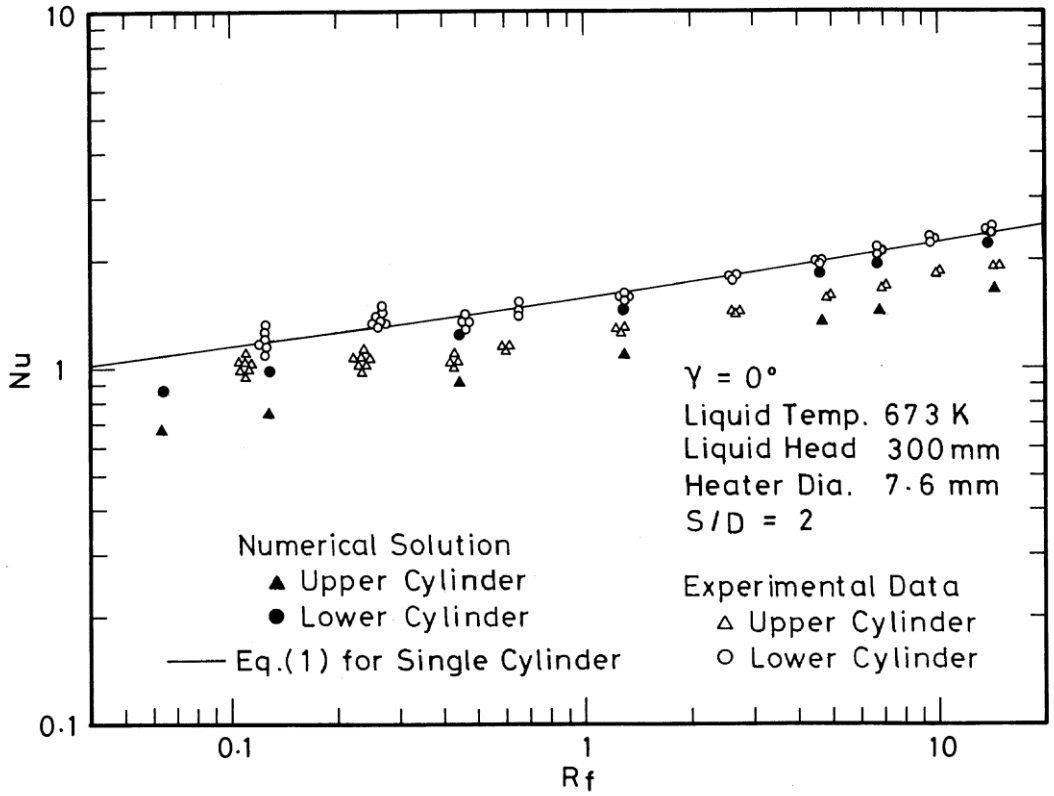

Figure 4. Experimental data of *Nu* for lower and upper cylinders at γ=0° compared with the theoretical solutions.

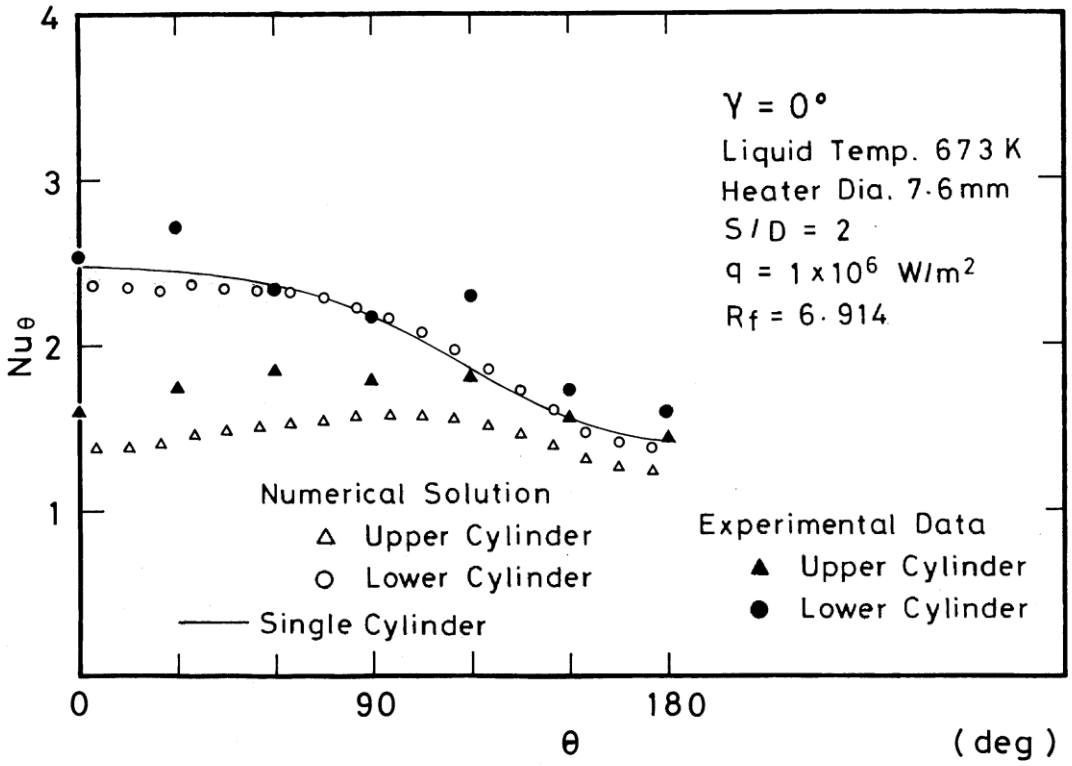

Figure 5. Comparison of Nu_θ data for γ=0° with the theoretical solutions.

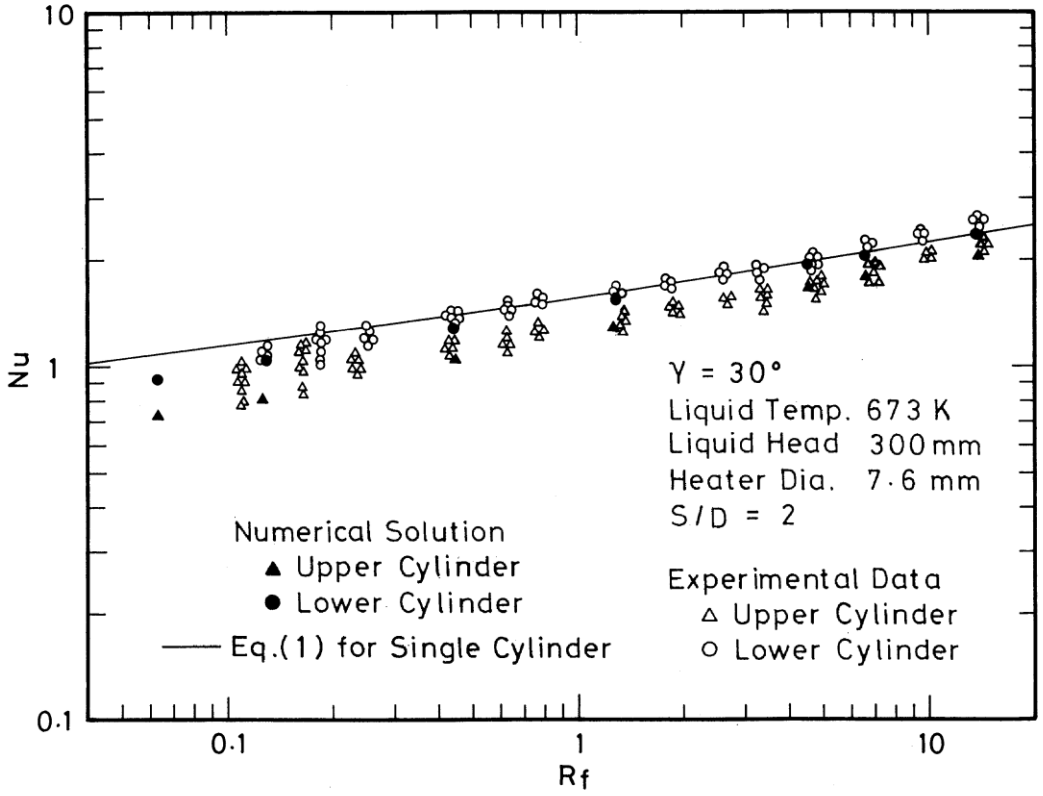

Figure 6. Experimental data of *Nu* for lower and upper cylinders at γ=30° compared with the theoretical solutions.

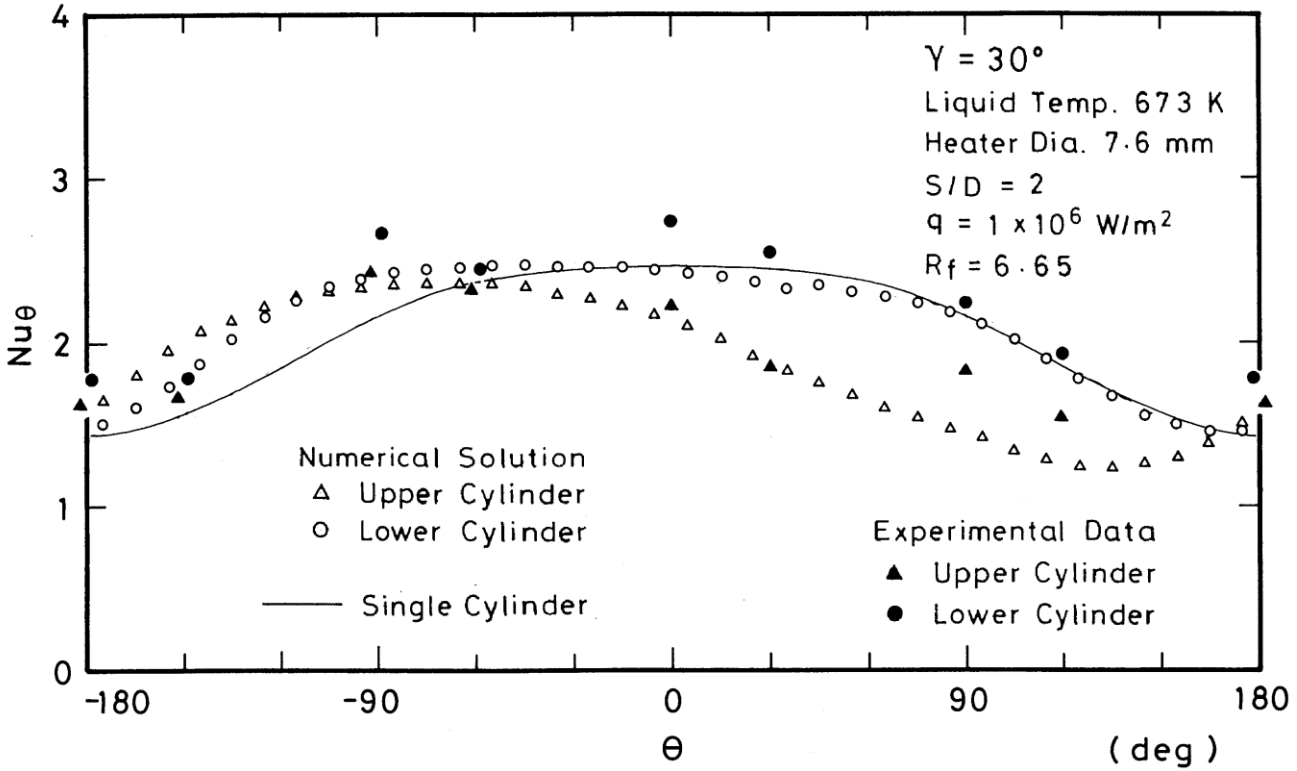

Figure 7. Comparison of Nu_θ data for γ=30° with the theoretical solutions.

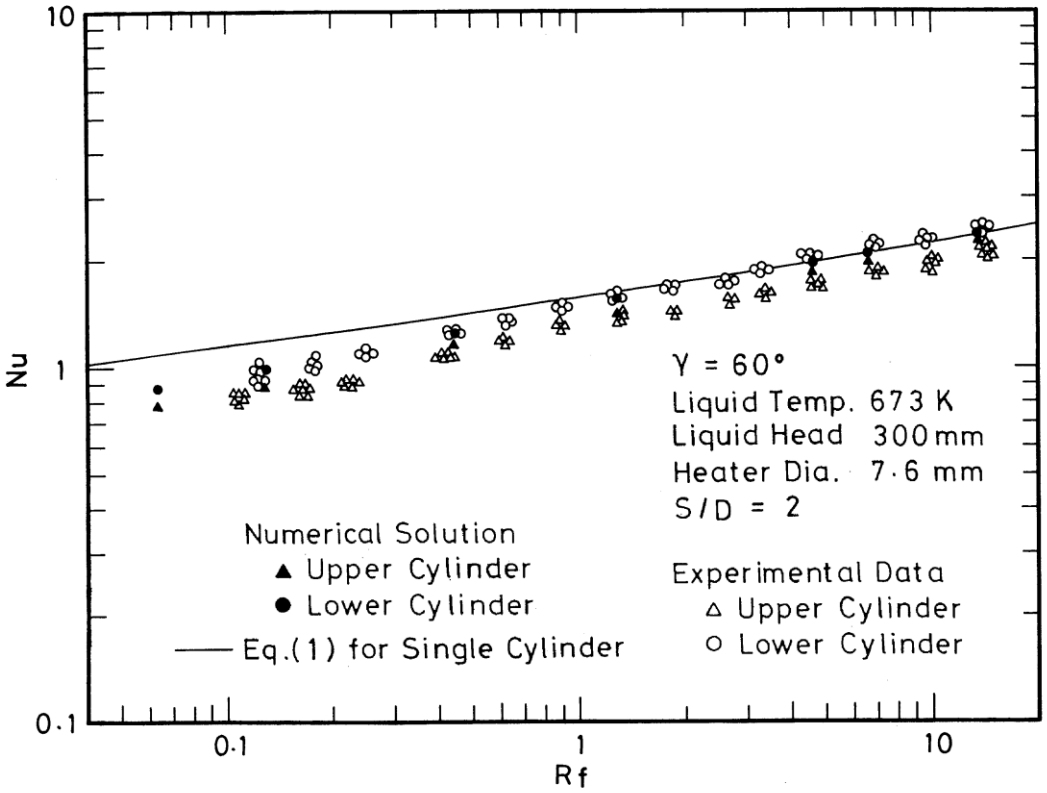

Figure 8. Experimental data of *Nu* for lower and upper cylinders at γ=60° compared with the theoretical solutions.

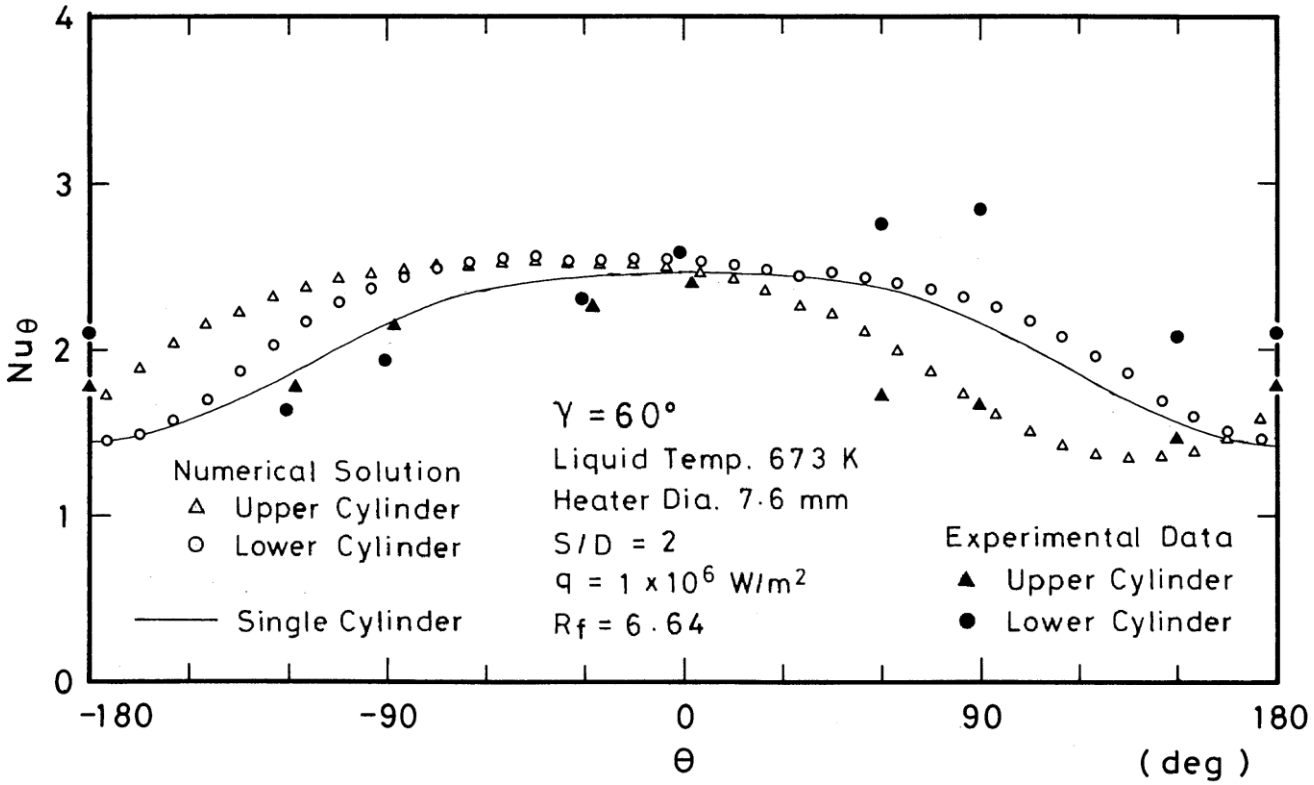

Figure 9. Comparison of Nu_θ data for γ=60° with the theoretical solutions.

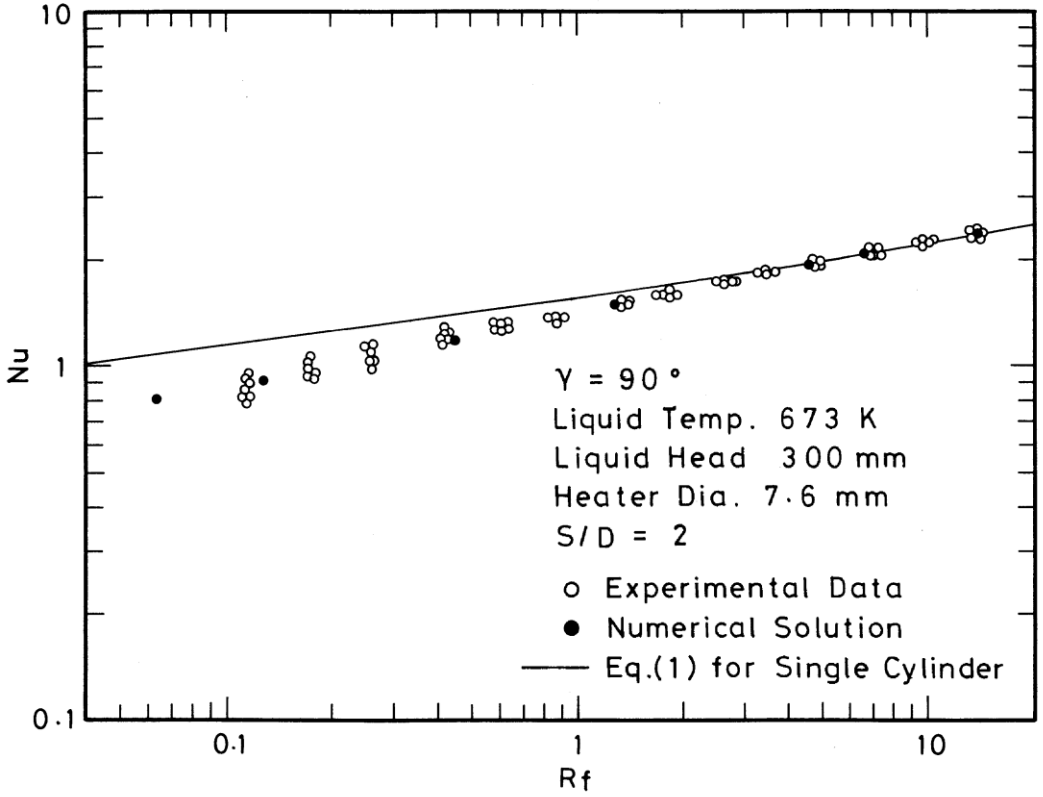

Figure 10. Experimental data of *Nu* for lower and upper cylinders at γ=90° compared with the theoretical solutions.

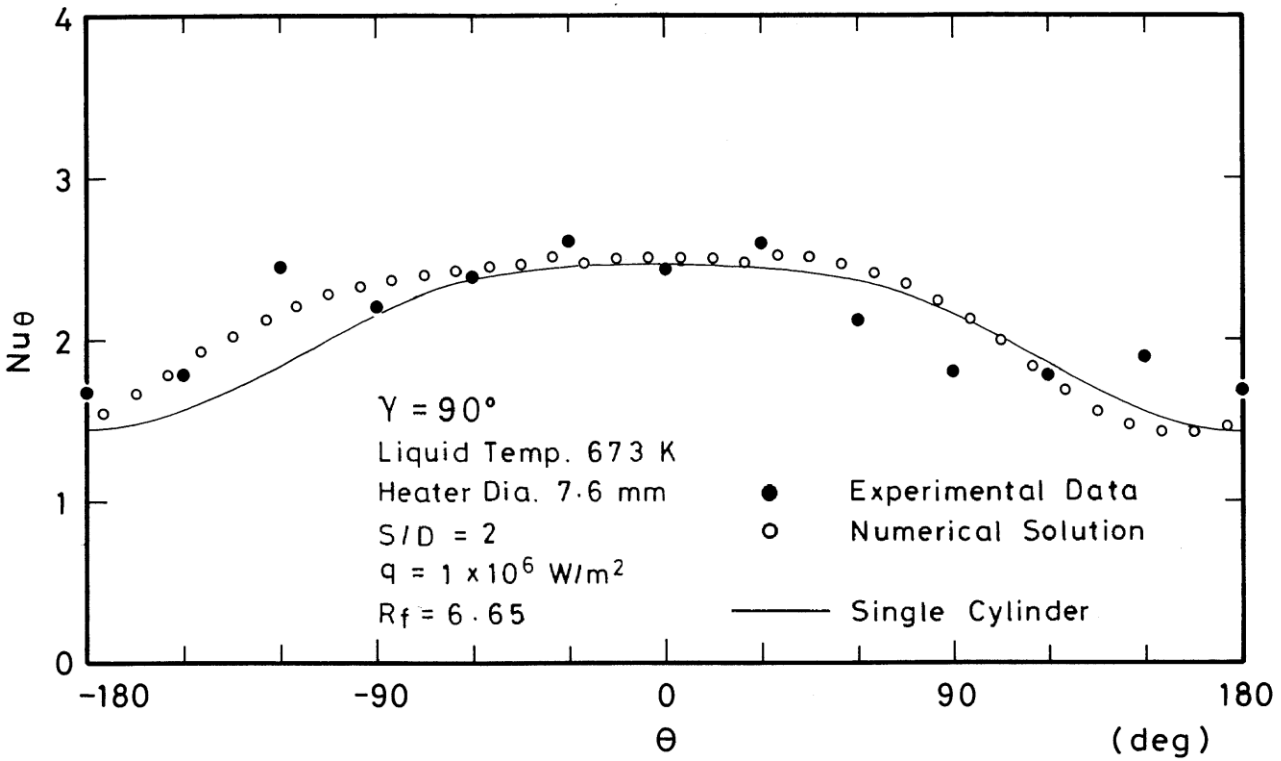

Figure 11. Comparison of Nu_θ data for γ=90° with the theoretical solutions.

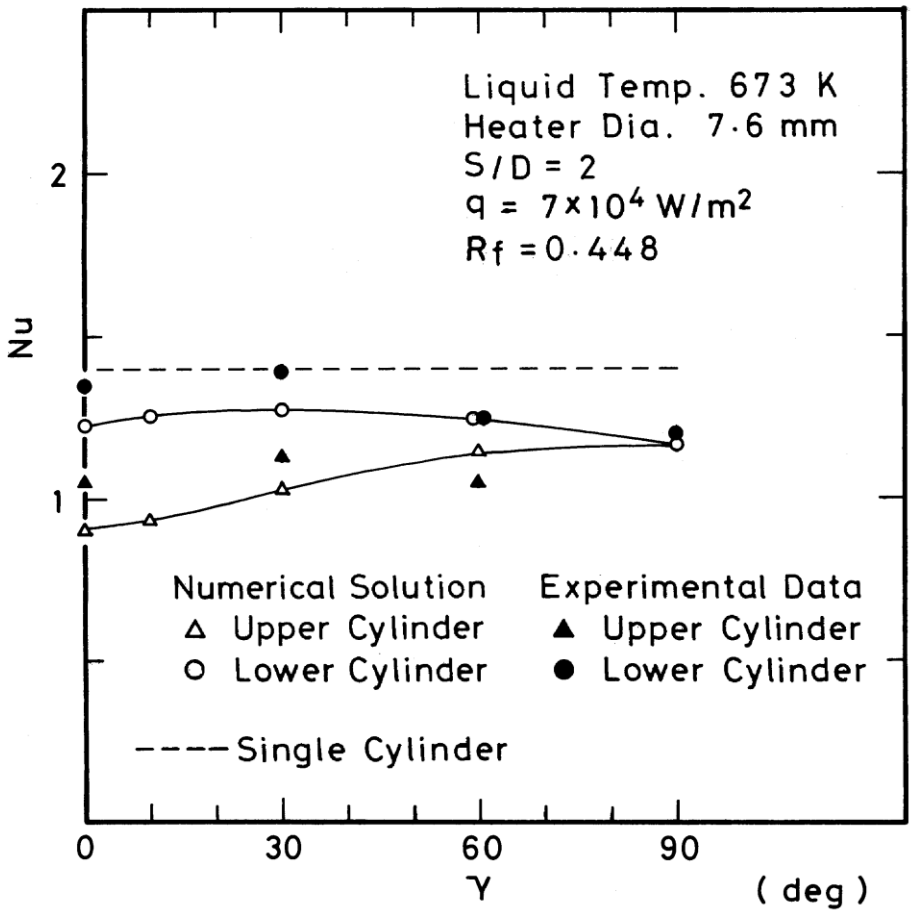

Figure 12 (a). Effect of setting angle on *Nu* for R_f=0.448.

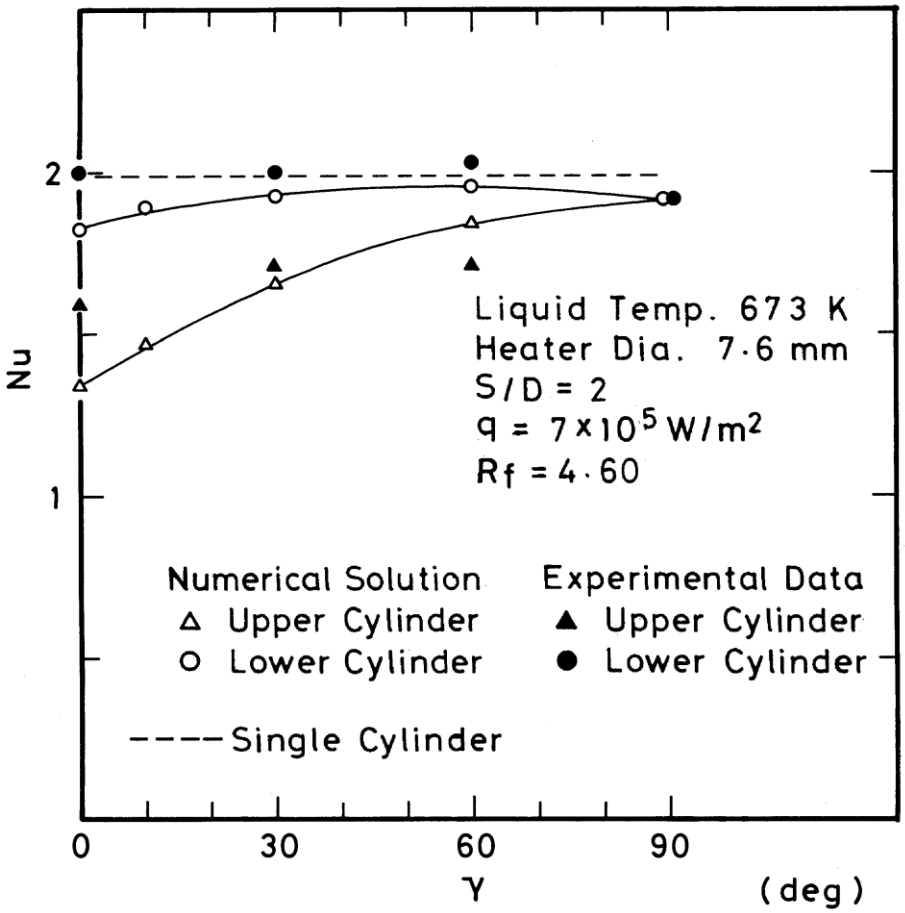

Figure 12 (b). Effect of setting angle on *Nu* for R_f=4.6.

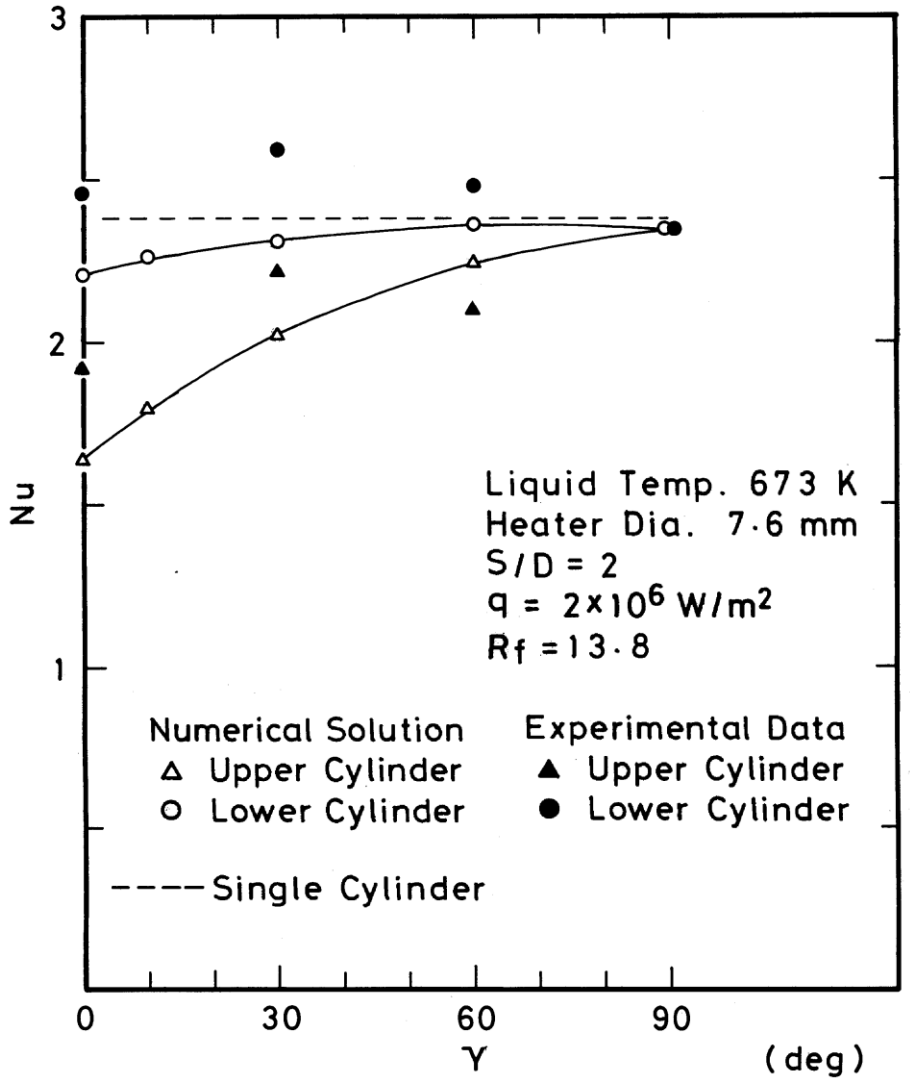

Figure 12 (c). Effect of setting angle on *Nu* for R_f=13.8.

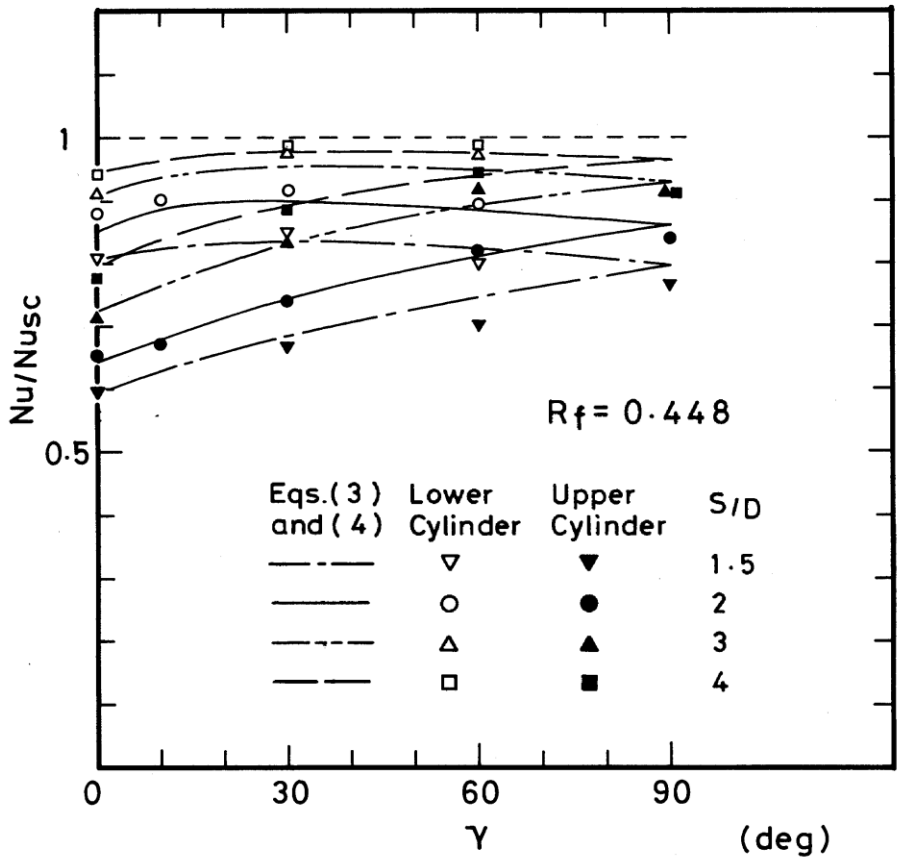

Figure 13 (a). Nu/Nu_{sc} versus γ for upper and lower cylinders with S/D as a parameter at R_f =0.448.

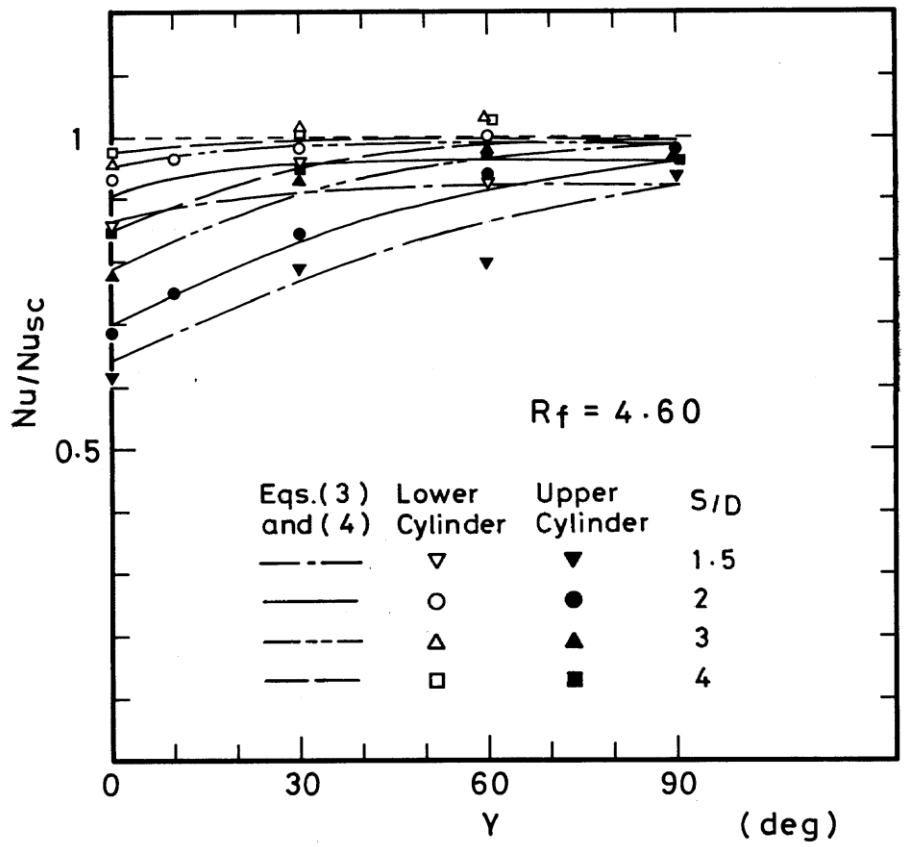

Figure 13 (b). *Nu/Nu*$_{sc}$ versus γ for upper and lower cylinders with *S/D* as a parameter at R_f=4.6.

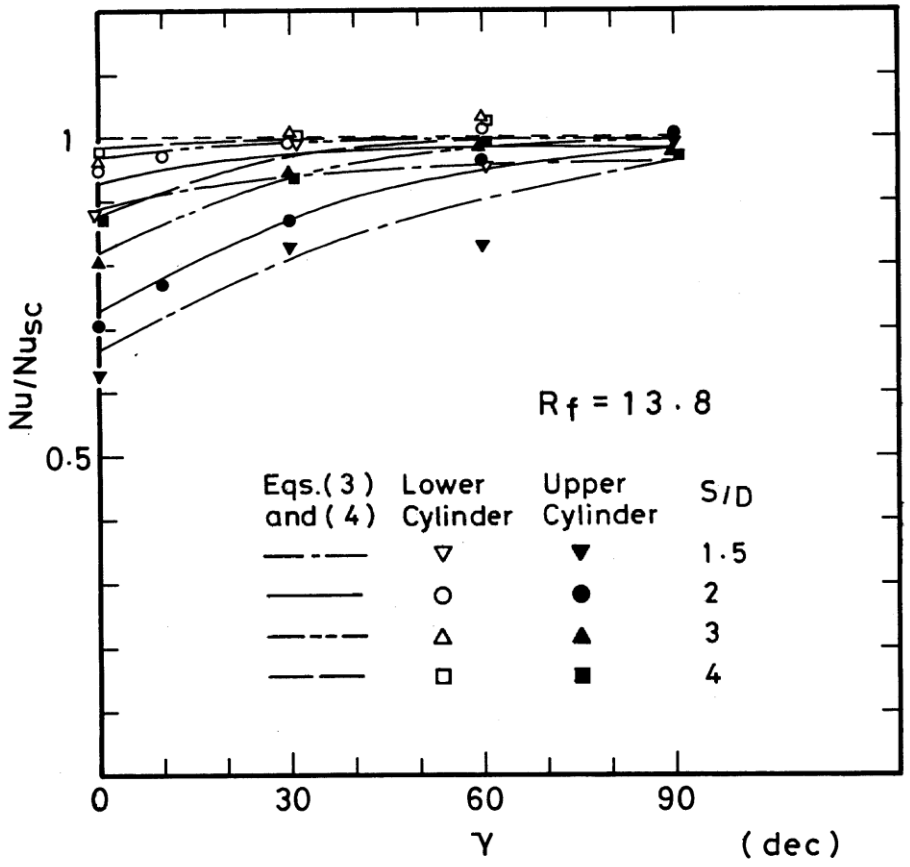

Figure 13 (c). *Nu/Nu*$_{sc}$ versus γ for upper and lower cylinders with *S/D* as a parameter at R_f =13.8.

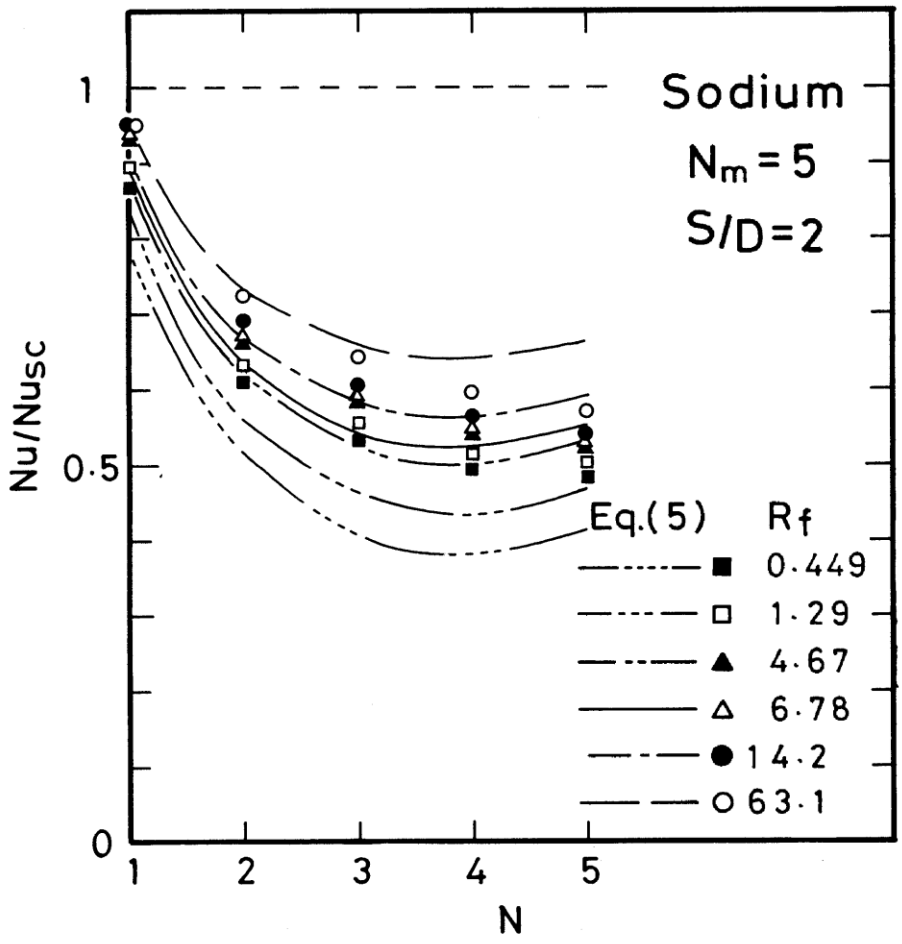

Figure 14. *Nu/Nu*$_{sc}$ versus cylinder number *N* for N_m=5 with R_f as a parameter. Comparison with the predicted curves.

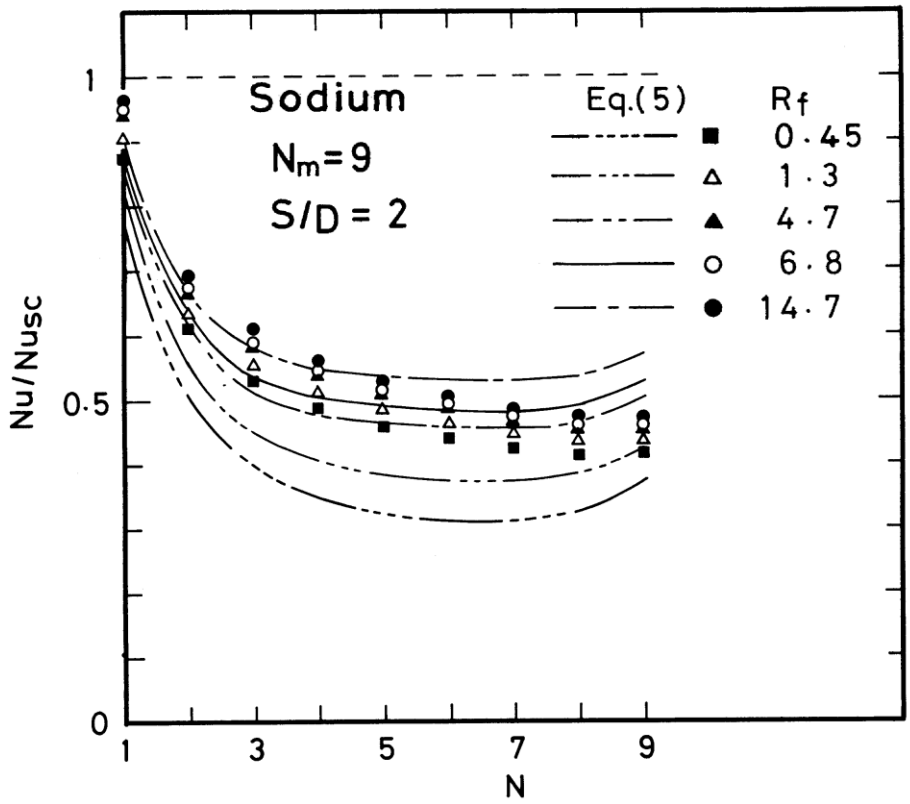

Figure 15. *Nu/Nu*$_{sc}$ versus cylinder number *N* for N_m=9 with R_f as a parameter. Comparison with the predicted curves.

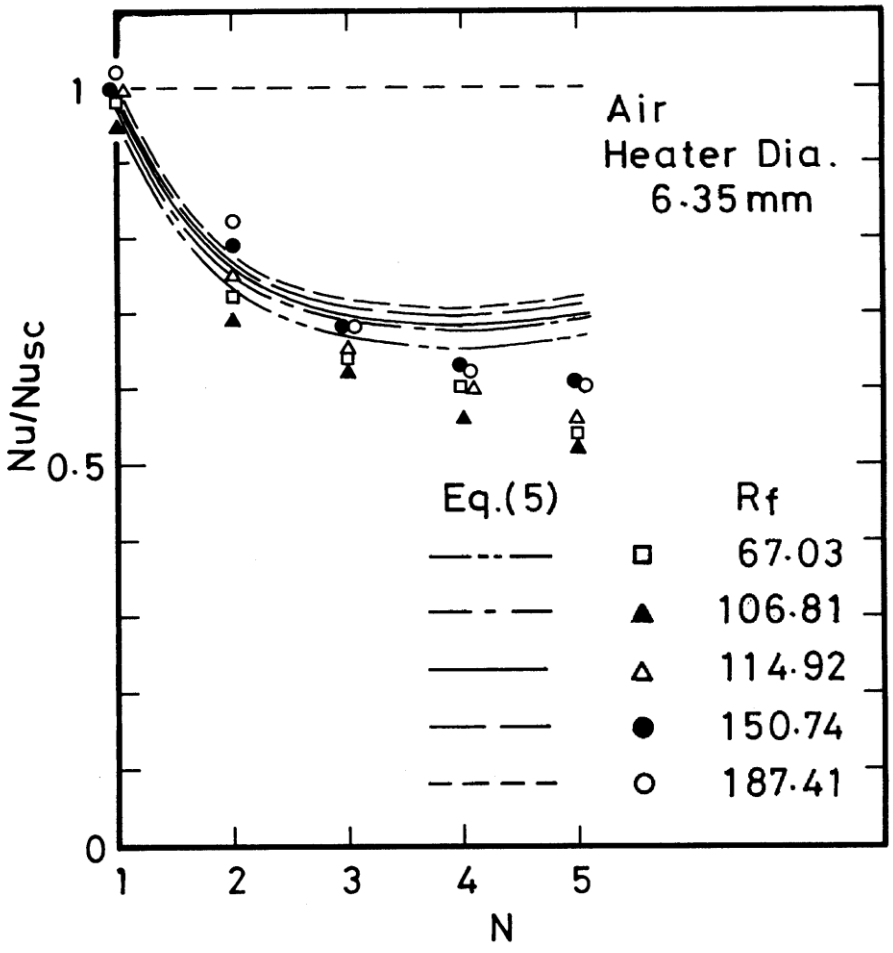

Figure16. Comparison of correlation with Marsters' experimental data on five cylinders in air.

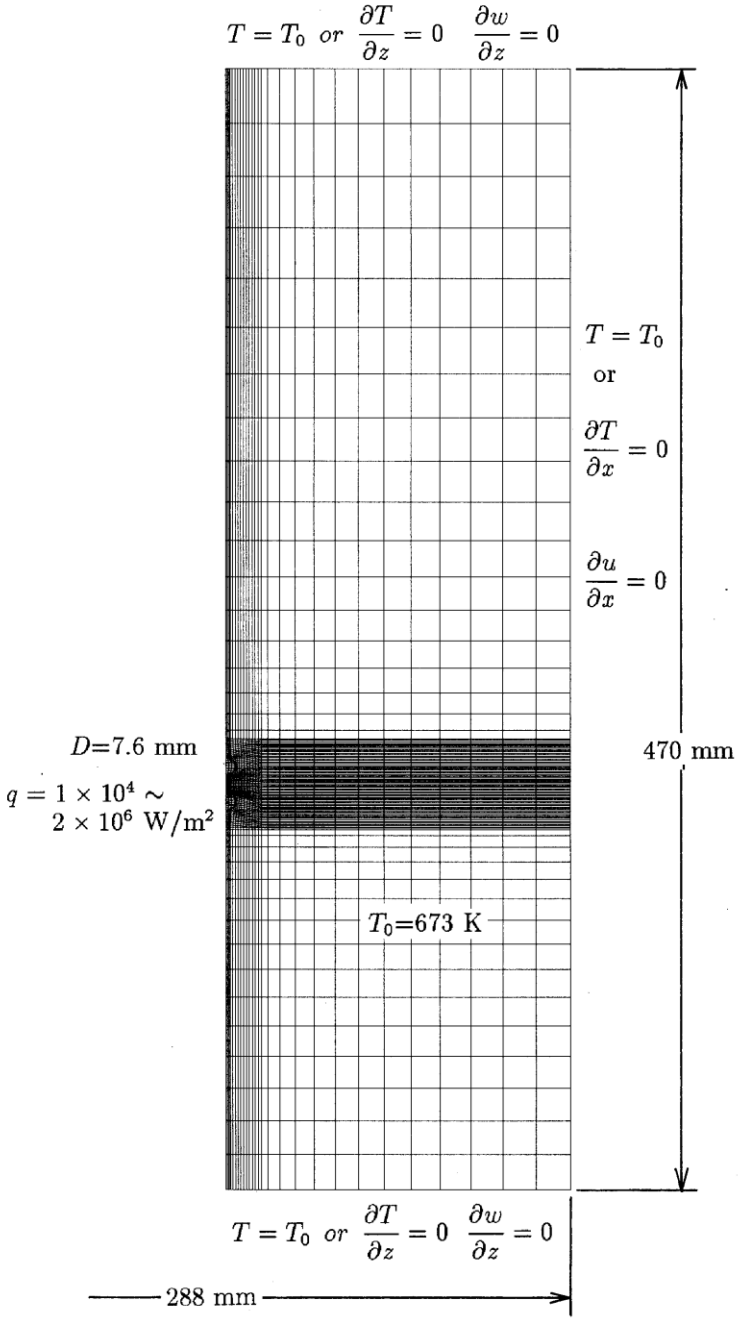

Figure 17 (a). Boundary fitted coordinates for γ=0°.

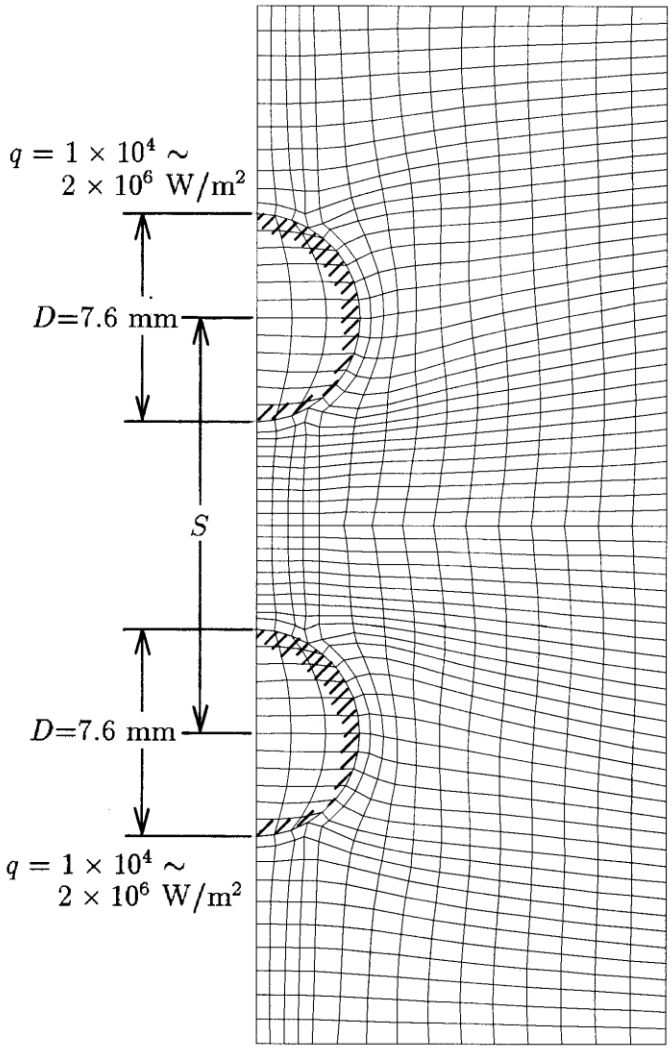

Figure17 (b). Details of Boundary fitted coordinates for γ=0°.

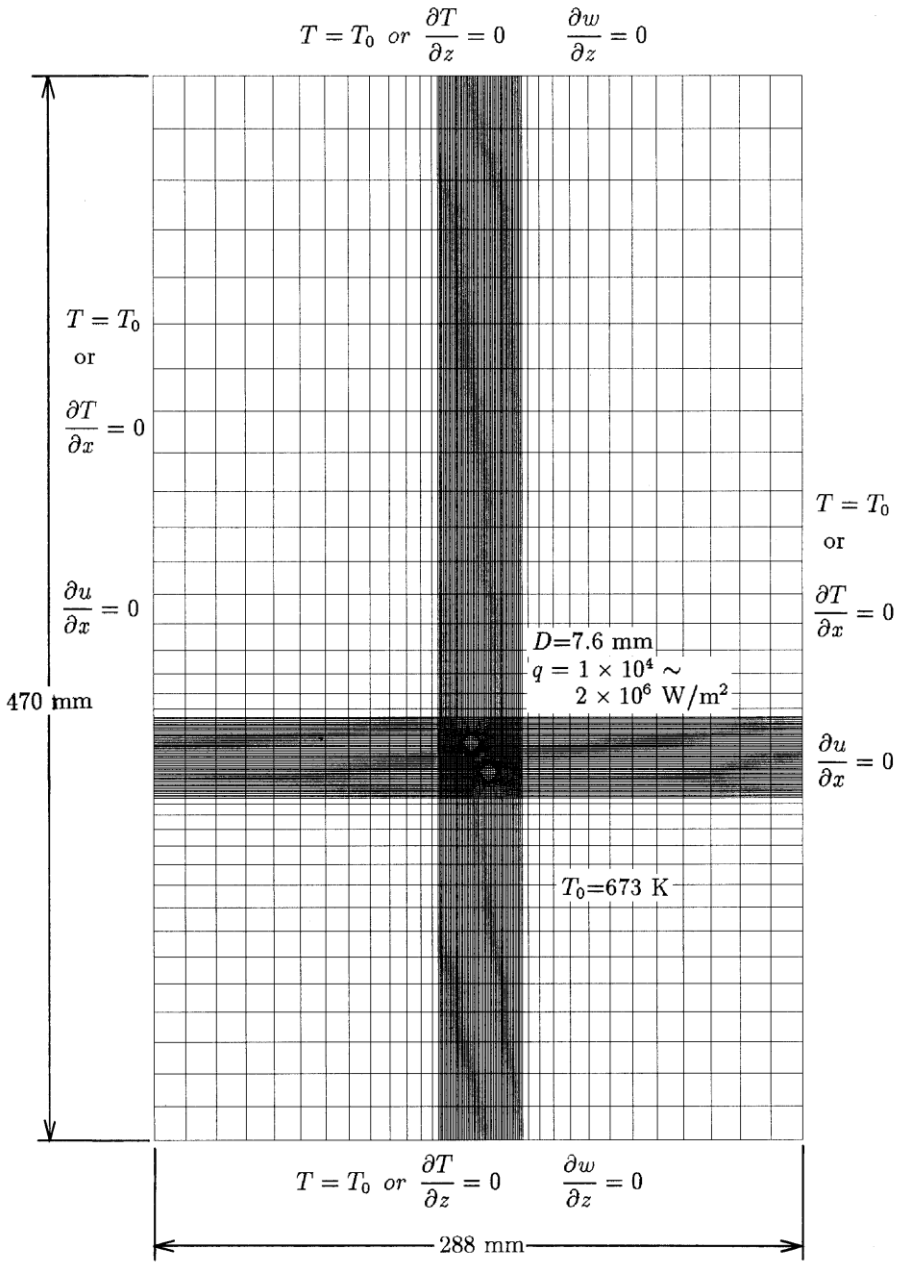

Figure 18 (a). Boundary fitted coordinates for γ=30°.

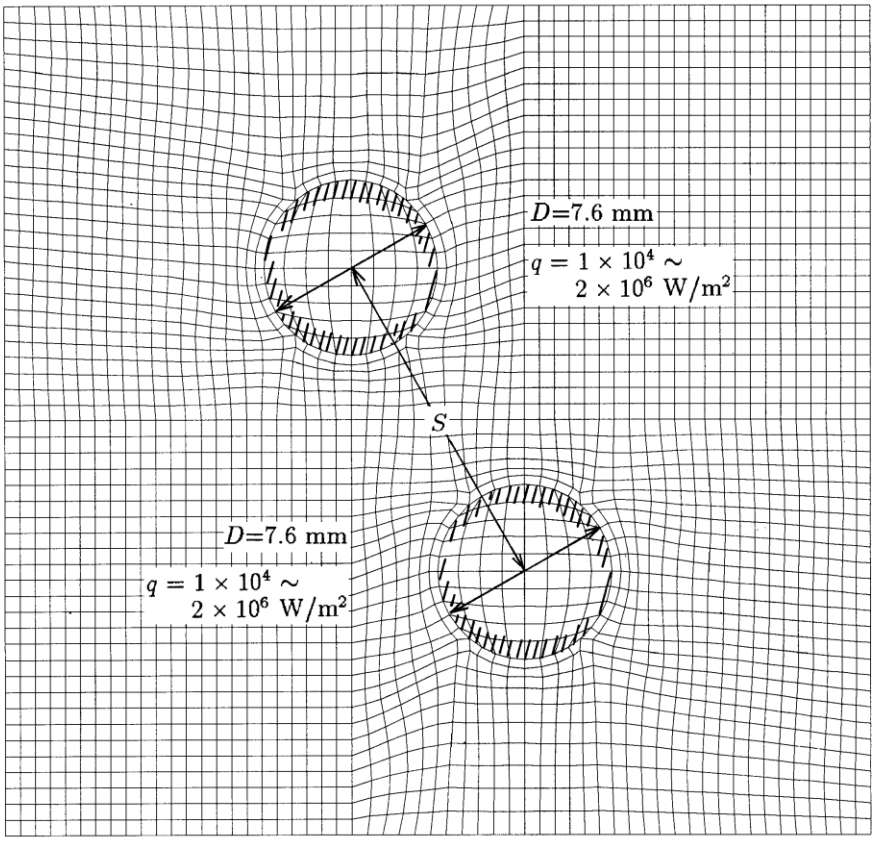

Figure 18 (b). Details of Boundary fitted coordinates for γ=30°.